Nuclear Science and Techniques (2026) 37:16
https://doi.org/10.1007/s41365-025-01853-7

Pulsed octupole magnet for beam instability mitigation in rapid cycling synchrotron

Liang-Sheng Huang[1,2,3] · Shou-Yan Xu[1,2] · Yun-Tao Liu[1,2] · Yi-Qin Liu[1,2] · Jian-Liang Chen[1,2] · Chang-Dong Deng[1,2] · Ming-Yang Huang[1,2] · Li Rao[1,2,3] · Han-Yang Liu[1,2] · Xin Qi[1,2,3]

Received: 25 December 2024 / Revised: 19 February 2025 / Accepted: 22 February 2025 / Published online: 9 December 2025

Abstract
The rapid cycling synchrotron (RCS) at the China spallation neutron source operates as a high-intensity proton accelerator. The coupled bunch instability was observed during RCS beam commissioning, which significantly limited the beam power. To investigate the dynamics of instability under an increased beam power, a pulsed octupole magnet with a gradient of 900 T/m^3 was developed. The magnet system integrated an octupole magnet with a pulsed power supply. The field was carefully measured to examine the performance before its installation into the tunnel. After the installation of the magnets, beam measurements were performed to confirm the effectiveness of the instability mitigation on an actual proton beam. The measurement results show that the instability can be suppressed using the pulsed octupole magnet, particularly at the high-energy stage in an acceleration cycle, meeting the requirements for stable operation of the accelerator. Additionally, when the instability is completely suppressed through chromaticity optimization, octupole magnets can significantly enhance the RCS transmission efficiency, which is crucial for controlling beam loss. The pulsed octupole magnet offers significant progress in beam stability in the RCS, providing valuable experience for further beam power enhancement.

Keywords China spallation neutron source · Rapid cycling synchrotron · Coupled bunch instability · Octupole magnet

1 Introduction

Octupole magnets have been extensively employed in ring accelerators to cure transverse instabilities, as evidenced by their applications in various facilities, including the photon factory electron storage ring at KEK [1] and the main ring at J-PARC [2] in Japan, LHC [3] at CERN in Switzerland, SIS100 synchrotron [4] in Germany, and BEPC [5] in China. The tune spread increases with the octupole field strength, thereby enhancing Landau damping. However, owing to the nonlinear feature of the field, the octupole magnet reduces the dynamic aperture [6], which restricts its power. Consequently, although instabilities have been successfully controlled [1, 2, 5], some accelerators, exemplified by the J-PARC main ring [2], face beam loss resulting from a reduced dynamic aperture post-instability suppression. Furthermore, the nonlinear dynamics of octupole magnets become increasingly complex under the influence of space charge effects, which may reduce the efficacy of Landau damping. Therefore, a comprehensive understanding of the application of octupole magnets for mitigating instabilities is crucial for the proton rapid cycling synchrotron (RCS), where the magnetic field changes rapidly and the beam size is relatively large [2, 7, 8].

The China spallation neutron source (CSNS) [9, 10] is a high-intensity proton accelerator-based facility. The accelerator complex comprises two main parts: a negative hydrogen (H^-) linac [11–13] and a RCS [7, 14]. The RCS is a four-fold

This work was supported by the Guangdong Basic and Applied Basic Research Foundation, China (No. 2021B1515140007).

✉ Liang-Sheng Huang
huangls@ihep.ac.cn

✉ Xin Qi
qix@ihep.ac.cn

[1] Spallation Neutron Source Science Center, Dongguan 523803, China

[2] Institute of High Energy Physics, CAS, Beijing 100049, China

[3] University of Chinese Academy of Sciences, Beijing 100049, China

structure lattice with a circumference of 227.92 m, including 24 dipole magnets and 48 quadrupole magnets. Each superperiod of the RCS consists of a straight section and an arc section. The RCS accelerates the proton beam from 80 MeV to 1.6 GeV at a repetition rate of 25 Hz. The designed beam power of the CSNS was 100 kW, corresponding to particles of $N_p = 1.56 \times 10^{13}$ per pulse. Beam commissioning of the RCS began in 2017. An unforeseen instability in the horizontal plane was first observed [15, 16], which has emerged as a critical challenge during beam commissioning. A series of measurements provided valuable insights and practical guidance for the instability mitigation. After 2 years of beam commissioning and a gradual power ramp-up, the RCS achieved a target beam power of 100 kW in February 2020. Currently, with the aid of AC sextupole magnets [17], trim quadrupole magnets [18] and 2nd harmonic cavities [19, 20], the beam power in the RCS has been increased to 170 kW, corresponding to $N_p = 2.65 \times 10^{13}$ particles per pulse. In Phase II of the CSNS (CSNS-II) [21], the beam power on the target will be upgraded to 500 kW, while the energy on the target remains unchanged (the RCS injection energy is increased to 300 MeV to mitigate space charge effects). This implies a substantial increase in beam intensity (equivalent to a particle number of $N_p = 7.8 \times 10^{13}$ per pulse). As the RCS beam intensity increased, the high-intensity effect became more severe. Notably, the instability observed during the beam commissioning at the CSNS presents a significant challenge for complete suppression at CSNS-II.

We investigated the potential of employing an octupole magnet to address the instability in the RCS; thus, a pulsed octupole magnet was proposed and developed in 2022. Following careful field measurements, the magnet system was seamlessly integrated into the accelerator during the summer of 2023. Extensive beam experiments were conducted in subsequent machine studies, including magnetic field calibrations and validation of instability suppression. These experiments yielded several positive results for suppressing instability, demonstrating the feasibility of using octupole magnets to mitigate instabilities in the RCS of CSNS.

This paper starts with a summary of RCS instabilities in Sect. 2, highlighting the requirement for octupole magnets to suppress the instability, as discussed in Sect. 3. Section 4 introduces the design of the magnet and its power supply as well as the magnetic field measurements in Sect. 5. Section 6 presents the beam measurements for instability mitigation. Detailed discussions on the application of octupole magnets in the RCS are provided in Sect. 7, followed by a summary of our conclusions.

2 Beam instability in the RCS

An unexpected instability was observed during the increase in the beam power from 20 to 50 kW in 2019, which worsened with further increases in the beam power. A series of comprehensive measurements [22] were undertaken to characterize the instability during a typical acceleration cycle, revealing that the issue is a coupled bunch instability. When the instability occurs, an oscillation of the beam position is observed in the transverse plane. The instability exhibits sensitivity to the tune, as illustrated in Fig. 3 in Ref. [23]. Variations in the tune lead to corresponding shifts in the timing of instability. We consider the case $\nu_x = 4.80$ as an example, as shown in Fig. 1, where the turn-by-turn (TbT) beam position in the horizontal plane and the transmission efficiency in the RCS dependence on the beam population are presented. Starting from the lowest bunch intensity, the horizontal beam position began to oscillate after injection. The oscillation amplitude increased as the beam intensity increased. The centroid's positive envelope on a logarithmic

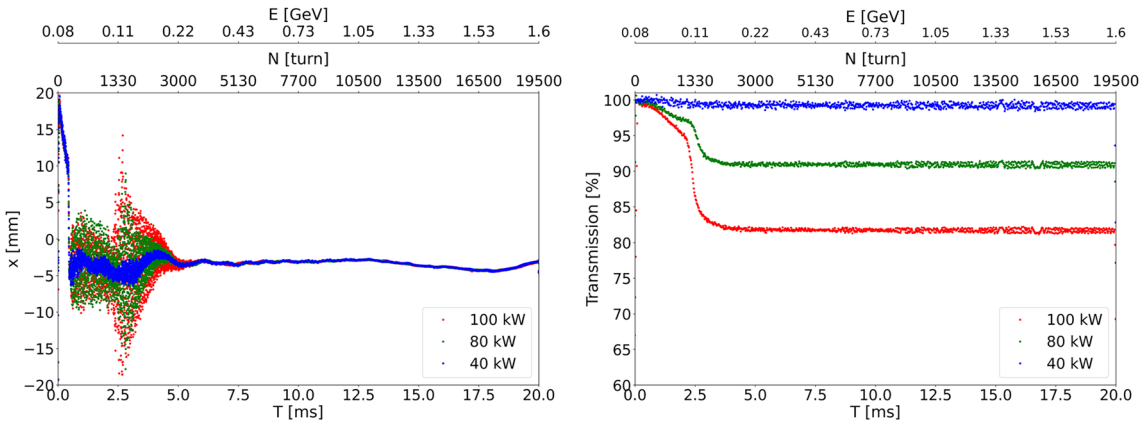

Fig. 1 (Color online) TbT beam position in the horizontal plane (left) and RCS beam transmission efficiency (right) vary with beam intensity under tune of (4.80, 4.86) with natural chromaticity. Red, green, and blue dots correspond to beam populations of 1.56×10^{13}, 1.25×10^{13} and 0.62×10^{13} per pulse, respectively

scale was linearly fitted and the growth time was provided. For a beam intensity of $N_p = 1.56 \times 10^{13}$ per pulse, which is equivalent to a beam power of 100 kW, the growth time was less than 1 ms. In the experiment, only one coupled mode was determined for the normal bunch mode (two bunches). The instability was first observed in the horizontal plane and subsequently appeared in the vertical plane as the beam power increased at $\nu_y > 4.86$. The coupled mode of the vertical instability is the same as that in the horizontal plane. The impedance study confirms that the instability is induced by the resonant impedance from the RF shield on the ceramic chamber [23, 24].

Comprehensive measurements provide valuable insights and practical guidance for mitigating the instability, such as tuning and chromaticity optimization. By applying the optimized tune and chromaticity, the instability was successfully suppressed at a beam power of 100 kW [15]. Following beam commissioning, the designed DC sextupole field was upgraded to an AC sextupole field [17]. This upgrade allows for dynamic control of chromaticity over the entire acceleration cycle, thereby simultaneously enhancing the beam transmission efficiency and suppressing instability. Consequently, the RCS transmission efficiency was significantly improved, and the instabilities were fully mitigated at a beam power of 170 kW.

Although the optimization of tune and chromaticity has been successfully implemented in the RCS, observations indicate that the beam power, using these two mitigation methods, reaches the threshold of instability. The approved upgrade of the CSNS-II aims to increase the beam power to 500 kW by increasing the number of particles in the RCS over the forthcoming years, which poses challenges for instability mitigation. Therefore, further studies are necessary to understand the dynamics of instability under increased beam power, including the proposal of new and effective mitigation strategies to ensure the designed beam power. Given their critical role in mitigating collective instabilities in numerous hadron synchrotrons [2–4], octupole magnets are a primary option for the RCS of the CSNS.

3 Requirement of octupole filed for the instability mitigation

Based on the classical calculation of the tune shift [25], the magnetic field of an octupole magnet in accelerators can be formulated as

$$B_y + iB_x = K_3(x + iy)^3, \tag{1}$$

where B_x and B_y represent the horizontal (x) and vertical (y) magnetic fields, respectively. For the particle rigidity $B\rho$ with a magnet length l, the octupole integrated strength is given by

$$K_3 = \frac{1}{6}\frac{k_3 l}{B\rho}, \tag{2}$$

with

$$k_3 = \frac{\partial^3 B_y}{\partial x^3}. \tag{3}$$

The horizontal and vertical magnetic fields in Eq. (1) are written as

$$B_x = K_3(3x^2y - y^3), \tag{4}$$

$$B_y = K_3(x^3 - 3xy^2). \tag{5}$$

Octupole magnets were used to control the tune shift in the transverse plane. Under reasonable simplifications [1, 26], the horizontal and vertical amplitude-dependent tune shifts are described as

$$\Delta Q_x = \frac{3}{8\pi}J_x \sum_i \beta_{x,i}^2 K_{3,i} - \frac{3}{4\pi}J_y \sum_i \beta_{x,i}\beta_{y,i}K_{3,i}, \tag{6}$$

$$\Delta Q_y = \frac{3}{8\pi}J_y \sum_i \beta_{y,i}^2 K_{3,i} - \frac{3}{4\pi}J_x \sum_i \beta_{x,i}\beta_{y,i}K_{3,i}, \tag{7}$$

where summation represents the sum across all magnets indexed by i. β_x and β_y are horizontal and vertical betatron functions, respectively. J_x and J_y denote actions in the transverse plane, and their average values are related to the beam emittance ϵ by $2\langle J\rangle = \epsilon$. As indicated by Eqs. (6) and (7), the amplitude-dependent tune shifts are likely to be linear functions of the octupole field strength. For an example estimation in the RCS of CSNS, let us assume four octupole magnets of identical strength K_3, with $\beta_x = \beta_y = 8$ m at magnets locations and $J_x \approx J_y = 30\,\pi$·mm·mrad, the tune shift is

$$\Delta Q_x = \Delta Q_y = -7 \times 10^{-4} \cdot K_3. \tag{8}$$

The required root mean square (RMS) frequency spread $\Delta\omega$ to suppress this instability can be expressed as [27]

$$\Delta\omega \geq (\Delta\omega)_{\mathrm{dyn}} \cdot \sqrt{\pi/2}, \tag{9}$$

with the dynamic part of the wake-induced betatron frequency shift $(\Delta\omega)_{\mathrm{dyn}}$, which relates to the growth time τ [28] of $(\Delta\omega)_{\mathrm{dyn}} = 1/\tau$. The growth time is assumed to be 0.5 ms, and the required frequency spread to suppress the instability is $\Delta\omega \geq 2.5 \times 10^3$ Hz. This implies that the tune shift must be greater than 0.005, requiring an integrated octupole field strength of $K_3 \approx 7$ T/m^2 to effectively mitigate instability.

To further investigate the efficacy of the octupole field in mitigating instability, we conducted 6D macroparticle tracking simulations using the existing code [29], which includes a representation of a single octupole magnet. A resonant wake from the ceramic chambers, as detailed in Table 1, is employed. The simplified physical model for the interaction between the beam and the wake field accumulates the wake force into a kick momentum. The macroparticles experienced the wake field effects at the interaction points in each revolution. To track the particle dynamics with energy ramping, the transfer matrix of synchrotron motion was included in the simulation. The tune shift caused by the octupole field was related to the transverse amplitude. The painting process in the RCS was included in the simulation, which made the beam distribution close to the realistic one. The TbT beam position oscillation with varying octupole strengths is shown in Fig. 2, clearly indicating a reduction in the oscillation amplitude as the octupole strength increases. Two tunes displaying the observed instability over the acceleration cycle were simulated at a beam power of 100 kW. These results clearly demonstrate the mitigating effect of the octupole field. Additionally, the simulation indicated an additional beam loss in the presence of the octupole field after mitigating the instability during the acceleration cycle. Therefore, the octupole magnetic field should be rapidly reduced to minimize the beam loss.

Table 1 Main parameters used in simulation

Parameter	Value
Bunch number	2
Beam power (kW)	100
Beam energy (GeV)	0.08–1.6
Res. impedance R_s (MΩ/m)	1
Res. frequency f_r (MHz)	0.12
Quality factor, Q	40
Wake decay time (turns)	500
Number of macroparticles	1×10^4

4 Design of pulsed octupole magnet

To dynamically control the tune spread over an acceleration cycle and minimize beam loss in the RCS, a pulsed octupole magnet is proposed. The required field gradient of the pulsed octupole magnet is related to the betatron function of the octupole magnet. Ceramic chambers must be used to mitigate the effects of eddy currents and ohmic losses [30]. These chambers are already employed in dipoles, quadrupoles, and injection painting magnets in the RCS, with little free space. The lattice in the RCS employs a triplet structure with four-fold symmetry [7]. This design effectively mitigates the effects of low-order structural resonance. In addition, existing magnets, including sextupole magnets [17], trim quadrupole magnets [18], and correctors [31], have successfully maintained this symmetry. Consequently, four octupole magnets were suggested. The location near quadrupole QF06 in every superperiod is shown in Fig. 3 and was chosen to accommodate the octupole magnets. This choice preserves the symmetry of the lattice and effectively utilizes the available ceramic chambers. The horizontal and vertical betatron functions at the location of octupole magnets were 8.3 m and 8.0 m, respectively. Based on the calculations shown in Fig. 2, K_3 was determined to be 20 T/m^2 in the low-energy stage. Considering a beam power of 500 kW at CSNS-II, the target K_3 value should be close to 100 T/m^2. As the energy increases, the strength of the octupole magnetic field required for instability suppression decreases. In the high-energy stage, a field gradient of $K_3 \approx 20$ T/m^2 is

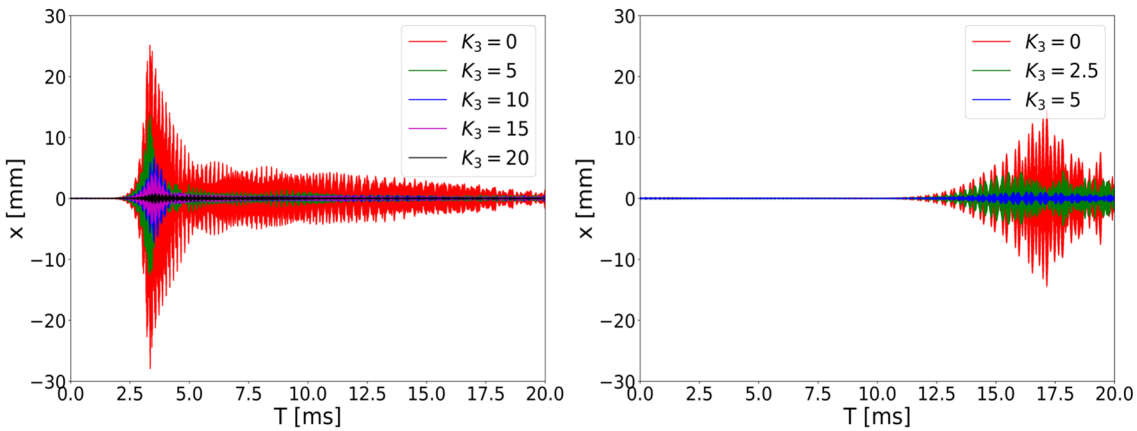

Fig. 2 (Color online) Simulated TbT beam position with the resonant wake in Table 1 in term of octupole field strength, where the beam power is 100 kW at tunes of $\nu_x = 4.80$ (left) and $\nu_x = 4.90$ (right), respectively

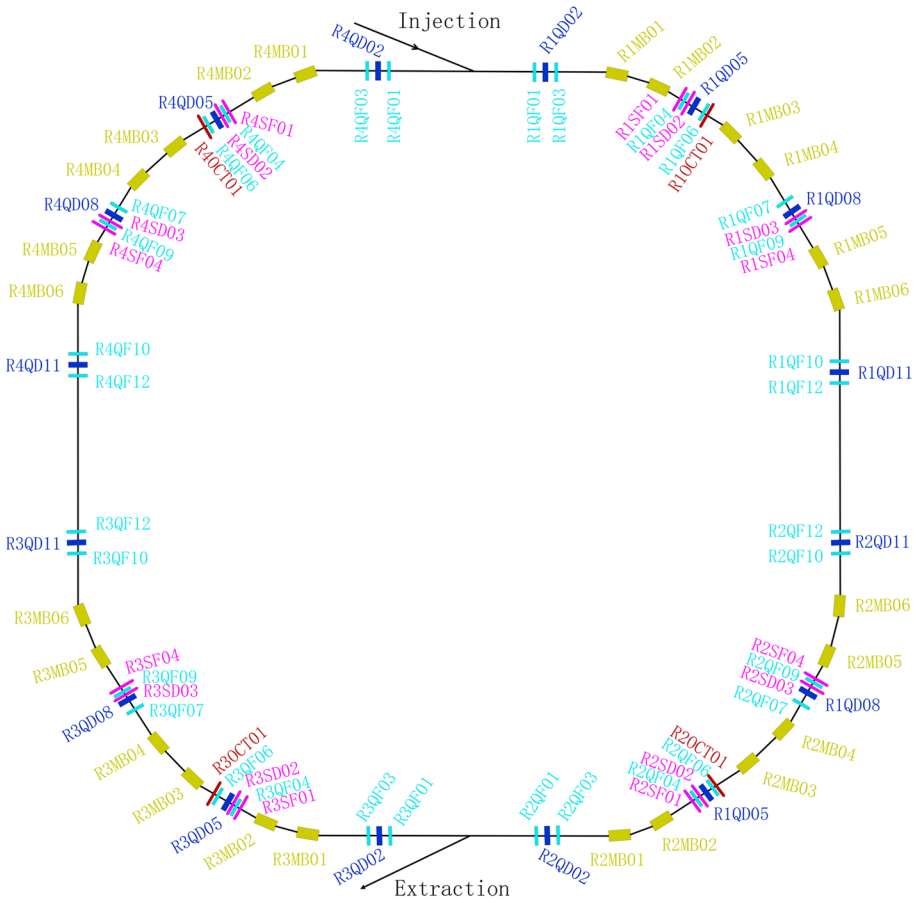

Fig. 3 (Color online) Magnet layout in the RCS, including four pulsed octupole magnets (dark red). The deep yellow, pink, cyan, and blue denote dipole, sextupole, focusing and defocusing quadrupole magnets

necessary to mitigate the instability completely. We set the target K_3 value to 45 T/m^2 at an injection energy of 300 MeV (equivalent to 15 T/m^2 at an extraction energy of 1.6 GeV) to reduce the manufacturing complexity of the octupole magnets. In this design, the octupole strength is insufficient to completely suppress the RCS instability. Nevertheless, it is adequate when used alongside existing mitigation strategies. This integral magnetic field translates into a field gradient of $k_3 = 900$ T/m^3. Table 2 lists the main parameters of the octupole magnets and power supply in the RCS. The octupole field switching was designed to be completed within 3 ms, with a field change rate of less than 210 T/m^3/ms.

Table 2 Main parameters of octupole magnets and power supply in the RCS

Parameter	Value
Magnet number	4
Effective length (mm)	200
Maximum field gradient k_3 (T/m^3)	900
Changing rate of field gradient (T/m^3/ms)	210
Aperture (mm)	256
Good field radius (mm)	118
High-order-Field error (%)	< 0.5
Self-inductance (mH)	4.6
Number of power supply	4
Maximum peak current (A)	620
Maximum peak voltage (V)	740
Changing rate of current (A/ms)	130
Current tracking error (%)	3

4.1 Octupole magnet

The magnet, characterized by a core length of 0.2 m and diameter of 256 mm, was designed to match the physical aperture in the RCS. Figure 4 displays a full 3D diagram of the octupole magnets and the 2D model with the distribution of the magnetic flux lines. The successful implementation of AC sextupole magnets [32] has provided valuable insights into the design and fabrication of pulsed octupole magnets. To enhance the mechanical rigidity of the magnet and facilitate the installation of the ceramic vacuum chamber, the pulsed magnet adopted an upper and lower half-in-one structure. The iron core is composed of 0.5 mm thick silicon steel insulated laminations, which were coated with B-stage epoxy resin. The endplate was constructed of stainless steel. The magnetic field was

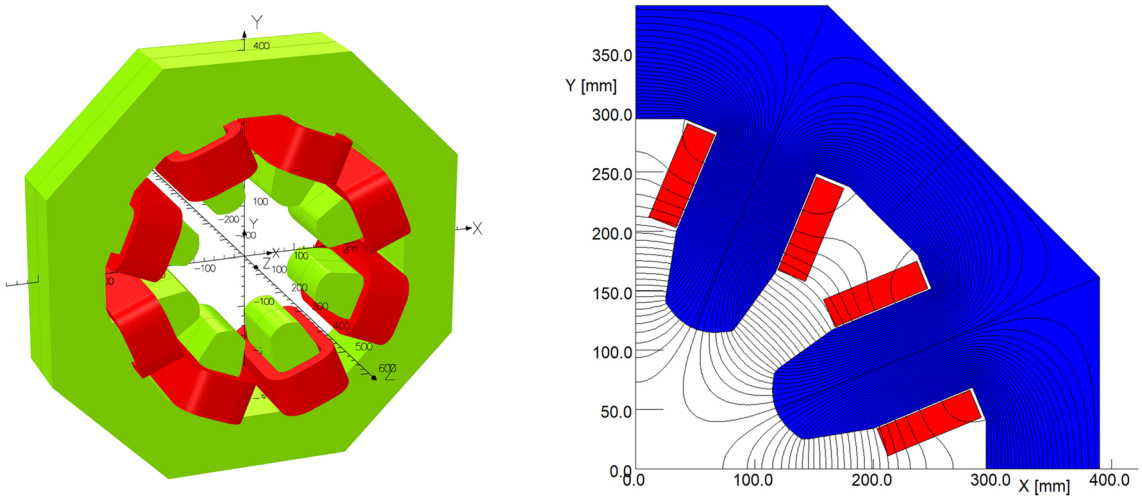

Fig. 4 (Color online) 3D diagram of octupole magnets (left) and 2D model with distribution of magnetic flux lines (right)

estimated after the pole chamfering and the total high-order field error was less than 0.5%. The excitation curve calculations revealed that the nonlinearity of the integral magnetic field was less than 3%. Each magnet was powered individually. To mitigate the voltage induced by the dynamic current, a 16-turn coil is selected to ensure that the corresponding induced voltage of the power supply is within an acceptable level.

The primary objective of the dynamic magnetic field simulation was to compute the eddy current distribution and temperature rise within the iron core of the magnets. To enhance the computational efficiency, a 1/8 core segment was utilized for analysis with the ELEKTRA/TR module in the OPERA software [33]. This approach enables the extraction of the magnetic field and other parameters at different excitation currents. A dedicated post-processing program was developed to process the calculation results. The average heat source density data obtained from the eddy current analysis were then imported into the TEMPO/ST module to calculate the temperature field, thereby determining the final temperature increase at various locations within the magnet core.

Following the setting of the material constants and parameters, a dynamic magnetic field was simulated. Figure 5 presents the reference curve of the magnetic field versus excitation current in the simulation. Over a 40 ms period, 200 output points were obtained with a convergence accuracy of 1×10^{-3} using a reasonable mesh grid. Eddy current effects in the iron core cause the magnetic field to change more slowly than the current, with a maximum time delay of approximately 0.2 ms. The peak eddy current reached 12 A, corresponding to the maximum rate of change in the excitation current. After slotting the endplate, the maximum recorded temperature rise was approximately 50 °C.

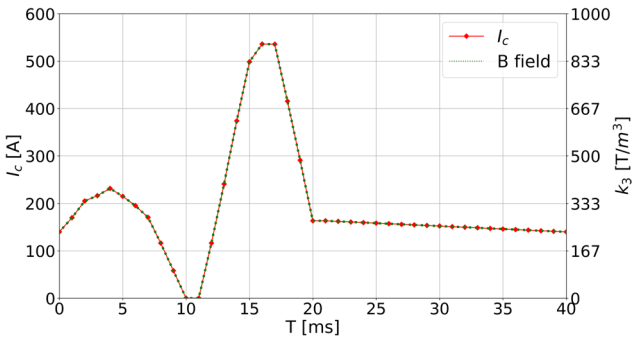

Fig. 5 (Color online) Designed curve of the magnetic field and excitation current for instability mitigation

4.2 Power supply

The octupole is powered individually by a programmable power supply, which is an essential component in precision applications where a high current and precise control are required. The maximum change rate is limited to 133 A/ms and corresponds to an excitation voltage of approximately 740 V, considering the magnet inductance. The maximum current was 620 A, which allowed for a margin. The power supply system utilizes a standardized modular switch-mode design, achieving a total output of ±740 V/±620 A through the series connection of standardized power modules. It comprises a front stage, an isolation transformation circuit, and a back stage. The front stage employs a soft-switching parallel resonant circuit to minimize switching interference and noise. The isolation transformation circuit enhanced the stability of the power supply. The back stage features an H-bridge chopper and an output filter, enabling bidirectional current and voltage outputs. With an equivalent switching

frequency of approximately 60 kHz, the system meets the demands for a rapid magnetic field shutdown. The power supply achieved a target stability of 0.2% and a current tracking accuracy of less than 3%. This stability level ensures that the power supply can deliver a steady current over prolonged periods. The power supply was synchronized with the CSNS 25 Hz timing, ensuring alignment with the dipole and octupole magnetic fields in the RCS. In addition, the system includes comprehensive fault and protection functions to ensure operational safety.

5 Field measurement

Before the magnet was installed in the RCS tunnel, field measurements were conducted to evaluate the performance of the magnet system, including both static and dynamic field measurements. These measurements ensured that the magnetic field conformed to the design specifications, thereby preventing potential alignment and operational issues.

5.1 Static field measurement

Static field measurements were performed to validate the physical design and manufacturing precision of the magnets. A Hall sensor [34] and a radial rotating coil [35] were employed in these measurements by utilizing a DC power supply. The repeatability of the Hall sensor was approximately 1×10^{-4}, whereas that of the radial rotating coil was better than 2×10^{-4}. The static magnetic field was measured up to 600 A, in increments of 10 A. Figure 6 shows the measured excitation curve of the center field gradient. At an excitation current of 514 A, the measured field is 900 T/m^3. The maximum measured center field is 1021 T/m^3 at 600 A. The measured results were in good agreement with the calculated values. The effect of core saturation is negligible, and the field gradient is directly proportional to the excitation current I with $k_3 = 1.751 \times I$. The effective length, derived from the measured center field gradient and the integrated field gradient, is 0.207 m. Furthermore, the dispersion of the integral magnetic field among the magnets was measured, and the results showed that the dispersion was less than 1.5%.

5.2 Dynamic field measurement

The purpose of the AC measurement of the magnets is to determine the dynamic response relationship between the current and the magnetic field, as well as the time delay induced by the excitation current waveforms. A stationary coil was used for the measurement. A timing clock was used to synchronize the acquisition of the current signal and the induced voltage signal of the magnetic field. The coil coefficient was calibrated using the Hall measurement results to enhance the measurement accuracy and obtain the absolute value of the integral magnetic field. During the measurement, the magnet was first powered by a sinusoidal current to heat it and reached a thermally stable state for approximately 2 h. Figure 7 shows the excitation current and integral magnetic field curves corresponding to the reference waveform in Fig. 5, in which only the beam acceleration period is presented. The magnetic field changes almost synchronously with the current curve with a time delay of approximately 0.2 ms during the acceleration cycle. In addition, different excitation current waveforms were employed, including triangular, trapezoidal, and sine waves. The maximum recorded time delay was approximately 0.3 ms. The repeatability of a given waveform is 0.1%.

Through rigorous measurements, the octupole magnet and its corresponding power supply demonstrated remarkable precision and stability. Consequently, we conclude that the magnet system complies with the design specifications,

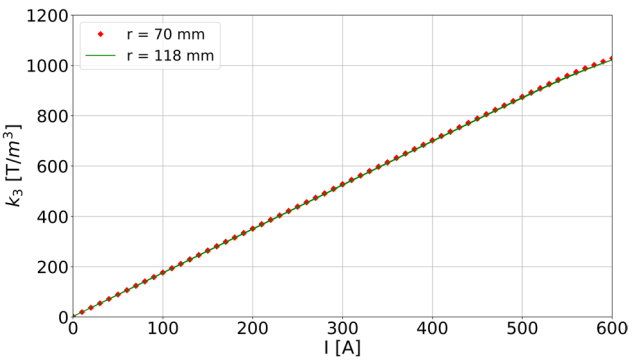

Fig. 6 (Color online) Excitation curve of the center octupole field gradient. The red diamond denotes the measured result at $r = 70$ mm, and the green line presents that at $r = 118$ mm

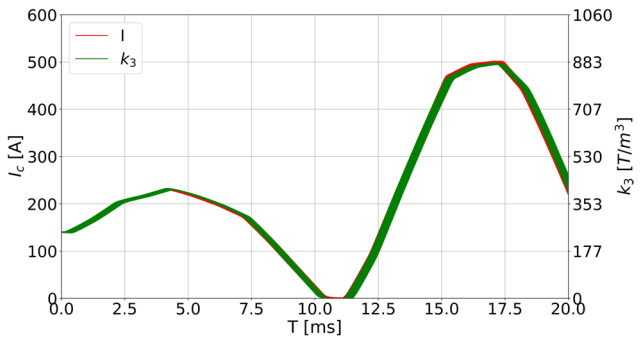

Fig. 7 (Color online) The response of the integrated magnetic field gradient to the excitation current over 30 trials. The red lines represent the excitation currents, and the green lines represent the integrated magnetic field gradients

providing essential data support for subsequent RCS applications.

6 Beam measurement of the instability

Following the installation of the magnets, a beam test with an octupole field was conducted promptly. Initially, critical magnetic field measurements with the beam were performed, including magnetic field alignment and synchronized measurements with RCS timing. Subsequently, extensive measurements were conducted to mitigate instability. Tunes play a significant role in the instability. The TbT bunch position was analyzed for the observed instability during the entire ramping process. The total number of particles was $N_p = 2.2 \times 10^{13}$ per pulse, corresponding to a beam power of 140 kW. Figure 8 shows the measured beam positions and beam populations with and without the optimized octupole field curve, including horizontal tunes of 4.80, 4.86, and 4.90, respectively. The oscillation amplitudes at the three distinct horizontal tunes displayed considerable variations, as shown in Fig. 8b–d. When the octupole magnet was off, instabilities were observed for all tunes. Using the optimized octupole field curve for different tunes, as shown in Fig. 8a, the instability can be entirely suppressed by the optimized field curve for all tunes, and the transmission efficiency is enhanced in the acceleration cycle. The results of this test confirm that the octupole magnet is effective in suppressing the RCS instability, as predicted.

In the operational tune with $\nu_x = 4.80$, the instability is successfully suppressed through chromaticity optimization [17]. Following this, we increased the strength of the octupole magnet to examine its impact on the beam. As illustrated in Fig. 9, with the optimized curve on the left, the octupole magnets further improved the RCS transmission efficiency on the right, which was not anticipated in the initial design. The applied octupole magnet strength is very weak, with $k_3 \approx 1\,\mathrm{T/m^3}$, as depicted in the left panel. We propose that this enhancement is due to the compensatory effects of the octupole magnets on the nonlinearities in the RCS. As a result, octupole magnets are employed in subsequent operations to increase transmission efficiency.

In the RCS, space charge effects are predominant during the low-energy phase, especially before 5 ms. As the beam energy increased, the space charge effects decreased. According to the existing literature [36], the strength of octupole magnets required to suppress instabilities increases significantly under strong space charge effects. For a bunched beam, the dynamics influenced by nonlinearities due to octupoles are complex, and thus, Landau

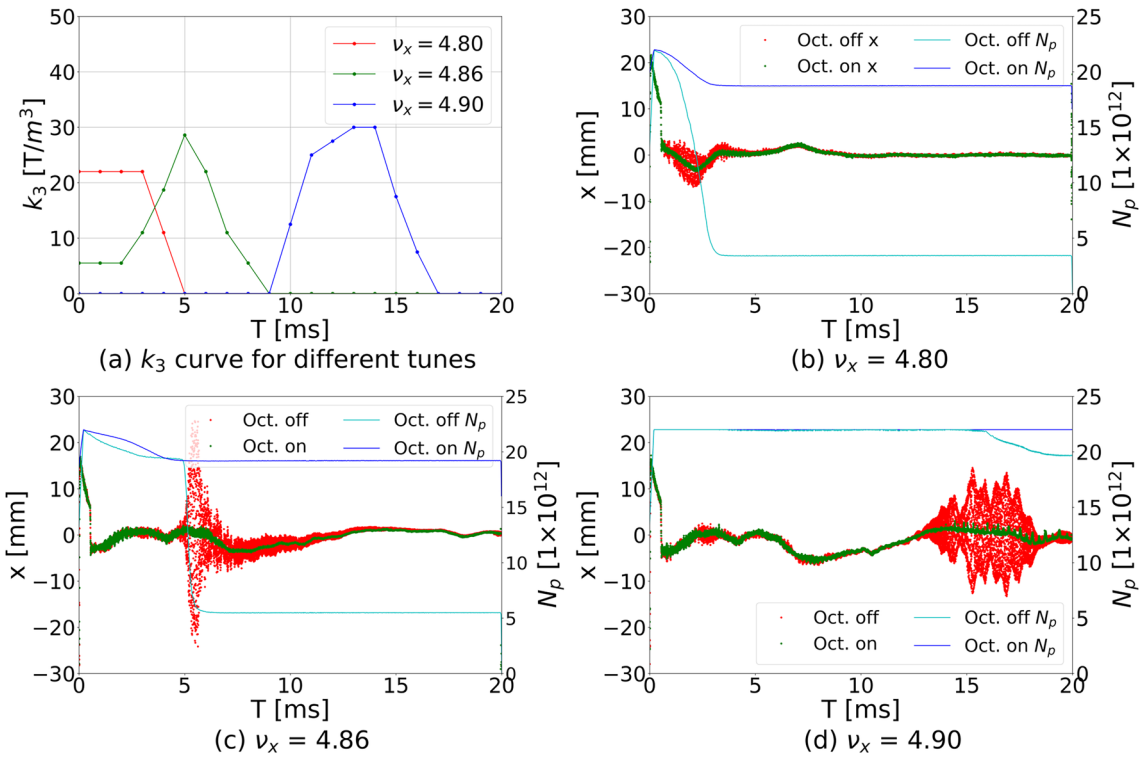

Fig. 8 (Color online) Experimental results of octupole magnet mitigation of instabilities at different timings. **a** shows the applied k_3 curves for different tunes. The TbT bunch positions and beam populations with and without the field curve depict for horizontal tune of 4.80 (**b**), 4.86 (**c**), and 4.90 (**d**), respectively

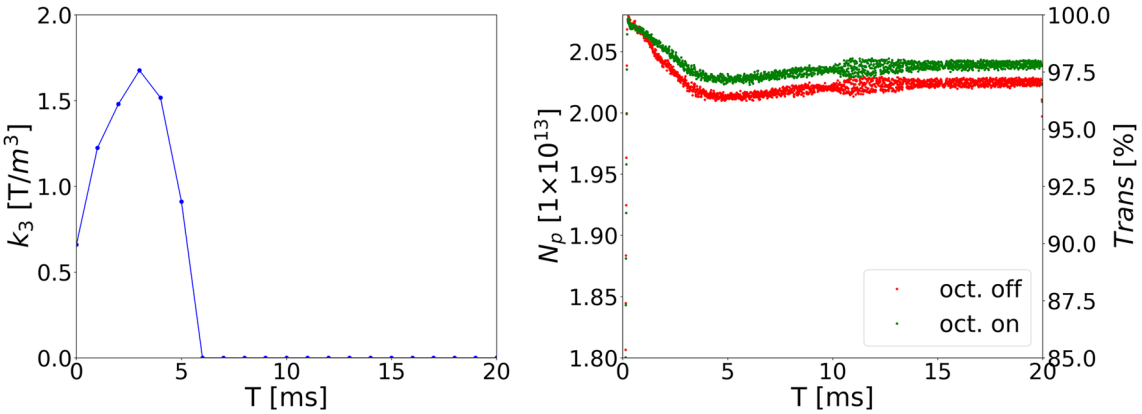

Fig. 9 (Color online) The RCS transmission efficiency (right) with and without the octupole field curve (left) in the operation. The instability is fully suppressed through chromaticity optimization in this case

Table 3 Growth time and required octupole strength to mitigate the RCS instability at different tunes

Parameter	Value	Value
ν_x	4.80	4.90
Instability observed time (ms)	2	14
Space charge tune shift	0.27	0.006
Growth time (ms)	3.2	4.5
k_3	16	6

damping cannot be adequately described by simplified dispersion relations [37]. This complexity was addressed in the present study through detailed measurements. As shown in Fig. 8, the instability was observed at different times depending on the tuning. Instability is observed in the low-energy stage, where space charge effects are strong at $\nu_x = 4.80$. Conversely, instability is observed in the high-energy stage with weak space charge effects at $\nu_x = 4.90$. This scenario allows for an experimental comparison of the impact of space charge effects on the coupled bunch instability. By setting the tunes to $\nu_x = 4.80$ and $\nu_x = 4.90$ at a beam power of 140 kW and adjusting the beam parameters to induce strong horizontal oscillations, the octupole magnet strength is incrementally increased to mitigate the instability until it is fully suppressed. The growth times of the instabilities and the corresponding octupole strengths are summarized in Table 3. The proportional calculation indicates that $k_3 = 8.4$ is required to suppress the instability with a growth time of 3.2 ms at $\nu_x = 4.80$. Compared to the instability occurring under weak space charge effects, the required octupole field strength significantly increases for RCS instability mitigation under strong space charge effects in Table 3.

7 Discussion

In the CSNS/RCS, octupole magnets have shown excellent performance in suppressing instability at the high-energy stage (approximately after 10 ms). They achieve complete suppression of the instability and maintain 100% transmission efficiency, thus meeting the requirements for long-term stable operation of the accelerator. Despite the effectiveness of octupole magnets in suppressing instabilities and improving the transmission efficiency at the low-energy stage, the RCS transmission efficiency remains inadequate for meeting operational demands (approximately 10% loss in Fig. 8). This is evident for the tunes of 4.80 and 4.86 in Fig. 9. At present, chromaticity optimization is primarily used to suppress instability and achieve a high RCS transmission efficiency during operation. Based on this, we performed tests to assess the impact of the octupole magnets on the transmission efficiency. The results showed that, as the strength of the octupole magnets increased, the transmission efficiency progressively decreased. An energy deviation for the RCS beam at injection was introduced to mitigate space charge effects [38]. The maximum momentum shift $\Delta p/p$ is close to 1%. To address the transmission efficiency issue, we performed a detailed analysis, including the 2nd chromaticity effects and dynamic aperture.

The octupole magnet is placed in the arc with dispersion function $D_x \approx 4.0$ m and the tune shift due to the 2nd order chromaticity [39] is expressed as

$$\Delta\nu = \frac{1}{8\pi} k_3 \beta D_x (\Delta p/p)^2, \tag{10}$$

with the beta function β. The 2nd chromaticity in the vertical plane is measured using a pulsed octupole magnet. The vertical tune was determined by acquiring the TbT bunch

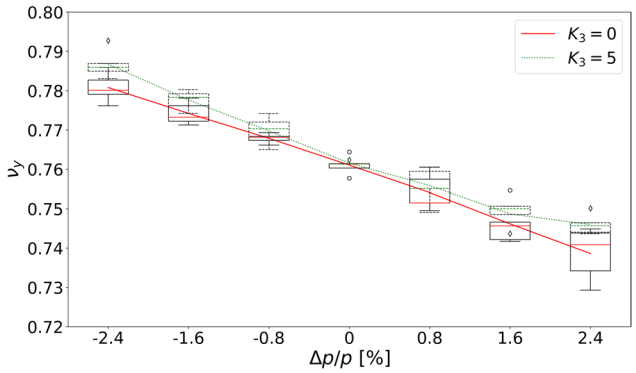

Fig. 10 (Color online) Measured tune in term of momentum shift with and without octupole magnet, where the red solid line represents the median line when the magnet OFF, while the green-dashed line indicates that when the magnet ON

position. An extraction kicker [40] was implemented to induce a visible oscillation in the vertical plane, providing better accuracy than the designed tune excitation [41]. Typically, tune measurements are conducted over 1024 turns at 11 ms and the timing of the vertical kicker can be adjusted to the moment of interest. The 2nd chromaticity was determined by fitting the tunes to the momentum shift, which was controlled by modulating the RF frequency. The measurements were performed at a low beam power of 20 kW. Figure 10 shows the measured tunes with and without the octupole field at different momentum shifts. For each momentum shift, measurements were performed five times. A box plot was provided to visualize the raw data, and the median difference between the two cases was fitted to determine the 2nd chromaticity. With momentum deviation $\Delta p/p$, the tune shift is inferred as $\Delta\nu_y \approx 10 \cdot (\Delta p/p)^2$. Notably, only the designed white noise excitation was used to measure the tuning in the RCS. The 2nd chromaticity in the horizontal plane was not measured because of the poor measurement accuracy with this white noise. Given similar horizontal and vertical beta functions at the octupole magnet, the 2nd chromaticity in the horizontal plane was assumed to be approximately equal to that in the vertical plane. Based on this calculation, the maximum tune shift due to the 2nd chromaticity in the RCS is approximately 0.001, which is significantly smaller than the space charge tune shift of 0.3 [42]. Consequently, the beam loss owing to the 2nd-order chromaticity can be ignored.

Utilizing a simplified lattice at a constant energy of 80MeV, we performed a comprehensive calculation of the dynamic aperture at various energy deviations, as depicted in Fig. 11. The chromaticity correction was implemented using a sextupole magnet. The cases of only chromaticity correction (a) and only an octupole field (c) are also presented for comparison. In the horizontal plane, the dynamic aperture is larger than the physical aperture of 60 mm for the case of only chromaticity correction (a), achieving a beam

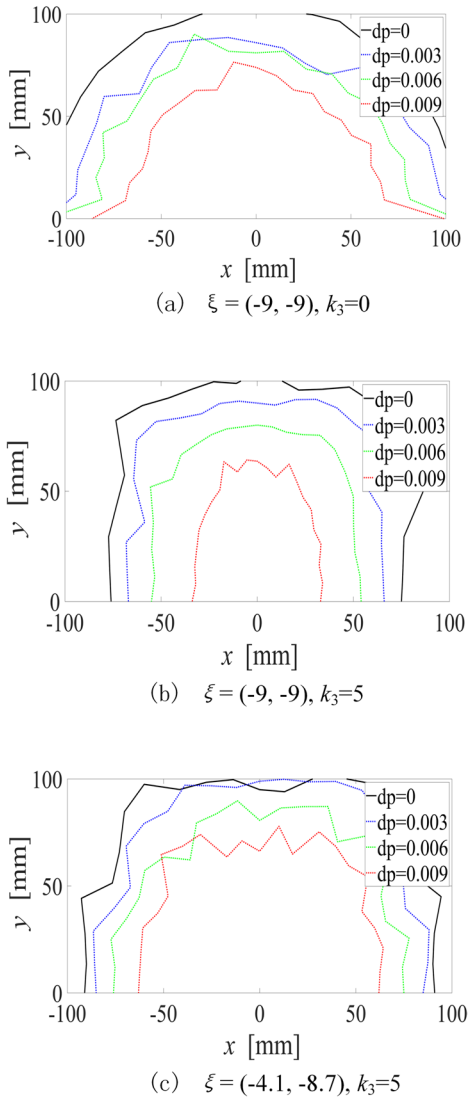

Fig. 11 (Color online) The dynamic aperture in term of $\Delta p/p$ (dp), where the tune is (4.80, 4.86) with constant energy of 80 MeV. **a** is optimized chromaticity and octupole off, **b** is optimized chromaticity of (−9, −9) and $k_3 = 5$, and **c** is natural chromaticity and $k_3 = 5$

transmission efficiency of approximately 100% in the actual operation. However, the dynamic aperture significantly diminished with octupole fields. The dynamic aperture notably decreases in the case of only an octupole field (c), particularly for the case of additional chromaticity correction (b). In the low-energy stage, both the beam size and momentum spread were relatively large. Under these conditions, even a weak octupole field can induce beam loss. As the beam energy increases, the beam size and momentum spread decrease. In the high-energy stage, the beam can sustain stability, even with a stronger octupole field. Consequently, it is essential to increase the dynamic aperture to improve the RCS transmission efficiency at the low-energy stage. A viable approach to restoring the RCS transmission efficiency

is to relocate the octupole magnets, which is a subject of our ongoing research.

8 Conclusion

The coupled bunch instability has been observed in the RCS of the CSNS. As the power levels increase in CSNS-II, more methods for suppressing this instability are being explored. One such method involves the use of octupole magnets to provide Landau damping. The pulsed octupole magnet system has been developed in the RCS. One octupole magnet is accommodated in every superperiod to preserve the lattice symmetry and efficiently use the existing ceramic chambers. Field measurements confirmed that the magnet satisfied the design values. After the installation of the magnet, preliminary instability measurements were performed. The instability was successfully suppressed by implementing the designed pulsed octupole magnets. At the high-energy stage, the instability can be fully suppressed using a pulsed octupole magnet without any additional beam loss, thereby meeting the requirements for long-term stable operation of the CSNS. However, at the low-energy stage, although the octupole magnet effectively suppresses the instability, the RCS transmission efficiency still falls short of operational conditions. This may be attributed to the reduction in dynamic aperture, necessitating further optimization to improve transmission efficiency, including the relocation of octupole magnets. Moreover, when the instability is completely suppressed through chromaticity optimization, octupole magnets can significantly enhance the RCS transmission efficiency, which is crucial for controlling beam loss during the current operations of the CSNS. More detailed measurements of instability mitigation should be conducted in future machine studies. Nevertheless, significant advancements in beam stability have been achieved in the preliminary measurements, providing valuable experience for further beam power enhancement.

Acknowledgements We extend our sincere gratitude to our colleagues in the Physics Group, the Magnet Group, the Power Supply Group, and the Mechanical Group of CSNS for their substantial support in the magnet design and field measurement. We also wish to thank our colleagues in the Beam Diagnosis and Operation Groups for their invaluable assistance during beam measurements.

Author contributions All authors contributed to the study conception and design. Simulations were conducted by Liang-Sheng Huang, Yun-Tao Liu, Yi-Qin Liu, and Chang-Dong Deng. The experiment was done by Liang-Sheng Huang, Shou-Yan Xu, Li Rao, and Han-Yang Liu. Data collection and analysis were performed by Liang-Sheng Huang and Jian-Liang Chen. This work was supported by Ming-Yang Huang and Xin Qi. The first draft of the manuscript was written by Liang-Sheng Huang, Yun-Tao Liu, and Chang-Dong Deng, and all authors commented on previous versions of the manuscript. All authors read and approved the final manuscript.

Data availability The data that support the findings of this study are openly available in Science Data Bank at https://cstr.cn/31253.11.sciencedb.j00186.00838 and https://doi.org/10.57760/sciencedb.j00186.00838.

Declarations

Conflict of interest The authors declare that they have no conflict of interest.

References

1. T. Miyajima, Y. Kobayashi, S. Nagahashi, Development of a pulsed octupole magnet system for studying the dynamics of transverse beam instabilities in electron storage rings. Nucl. Instrum. Methods Phys. Res. A. **581**, 589–600 (2007). https://doi.org/10.1016/j.nima.2007.08.120
2. S. Igarashi, A. Ando, T. Koseki, Octupole magnets for the instability damping at the J-PARC main ring, in *Proceedings of IPAC'12*, New Orleans, Louisiana, USA, WEPPR052, 3045-3047 (2012)
3. X. Buffat, W. Herr, N. Mounet et al., Stability diagrams of colliding beams in the Large Hadron Collider. Phys. Rev. Accel. Beams **17**, 111002 (2014). https://doi.org/10.1103/PhysRevSTAB.17.111002
4. P. Spiller, U. Blell, L. Bozyk et al., Status of the FAIR Heavy Ion Synchrotron Project SIS100, in *Proceedings of IPAC'15*, Richmond, VA, USA, THPF015, 3715-3717 (2015). https://doi.org/10.18429/JACoW-IPAC2015-THPF015
5. Q. Qin, Z. Guo, H. Huang et al., Electron cloud instability experiments on the BEPC. Nucl. Instrum. Methods Phys. Res. A. **547**, 239–248 (2005). https://doi.org/10.1016/j.nima.2005.02.027
6. S. Y. Lee, Accelerator Physics 2nd ed. World Scientific, Singapore, 64 (2004)
7. S. Wang, S.X. Fang, S.N. Fu et al., Introduction to the overall physics design of CSNS accelerators. Chin. Phys. C **33**(S2), 1–3 (2009). https://doi.org/10.1088/1674-1137/33/S2/001
8. Y. Shi, M. Zhang, L. Ou-Yang et al., Design of a rapid-cycling synchrotron for flash proton therapy. Nucl. Sci. Tech. **34**, 145 (2023). https://doi.org/10.1007/s41365-023-01283-3
9. China Spallation Neutron Source. Available at http://english.ihep.cas.cn/csns, date last accessed July 24, (2024)
10. J. Wei, H.S. Chen, Y.W. Chen et al., China Spallation Neutron Source: Design, R &D, and outlook. Nucl. Instrum. Methods Phys. Res. A. **600**, 10–13 (2008). https://doi.org/10.1016/j.nima.2008.11.017
11. H. Liu, J. Peng, K. Gong et al., The design and construction of CSNS drift tube linac. Nucl. Instrum. Methods Phys. Res. A. **911**, 131–137 (2018). https://doi.org/10.1016/j.nima.2018.10.034
12. J. Peng, Y. Han, Z. Li et al., Beam dynamics studies for the CSNS due to a quadrupole fault, in *Proceedings of LINAC'18*, Beijing, China, TUPO114, 573-575 (2018). https://doi.org/10.18429/JACoW-LINAC2018-TUPO114
13. J. Peng, Y. Han, Z. Li et al., Beam loss studies in the CSNS Linac, in *Proceedings of HB'23*, Geneva, Switzerland, WEA4C1, 297-299 (2023). https://doi.org/10.18429/JACoW-HB2023-WEA4C1
14. S. Wang, S. Fu, H. Qu et al., Development and commissioning for high-intensity proton accelerator of China Spallation Neutron Source. Atom. Energy Sci. Technol. **56**(9), 1747–1759 (2002). https://doi.org/10.7538/yzk.2022.youxian.0591. ((**in Chinese**))
15. S. Xu, H. Liu, J. Peng et al., Beam commissioning and beam loss control for CSNS accelerators. JINST **15**, P07023 (2020). https://doi.org/10.1088/1748-0221/15/07/P07023

16. L. Huang, S. Xu, S. Wang, The characteristic of the beam position growth in CSNS/RCS, in *Proceedings of IPAC'21*, Campinas, Brazil, TUPAB262, 630–632 (2021). https://doi.org/10.18429/JACoW-IPAC2021-TUPAB262
17. L. Huang, Y. An, C. Deng et al., Upgrade of the sextupole field for beam instability mitigation in rapid cycling synchrotron of China Spallation Neutron Source. Radiat. Detect. Technol. Methods **7**, 550–560 (2023). https://doi.org/10.1007/s41605-023-00428-7
18. Y. Li, Y. Yuan, S. Xu et al., Half-integer resonance caused by dc injection bump magnets and superperiodicity restoration in high-intensity hadron synchrotrons. Phys. Rev. Accel. Beams **26**, 104201 (2023). https://doi.org/10.1103/PhysRevAccelBeams.26.104201
19. B. Wu, X. Li, Z. Li et al., Development of a large nanocrystalline soft magnetic alloy core with high μ_p'Qf products for CSNS-II. Nucl. Sci. Tech. **33**, 99 (2022). https://doi.org/10.1007/s41365-022-01087-x
20. J. Wu, X. Li, B. Wu et al., Design and commissioning of a wideband RF system for CSNS-II rapid-cycling synchrotron. Nucl. Sci. Tech. **35**, 5 (2024). https://doi.org/10.1007/s41365-022-01087-x
21. H. Liu, S. Wang, Longitudinal beam dynamic design of 500 kW beam power upgrade for CSNS-II RCS. Radiat. Detect. Technol. Methods **6**, 339–348 (2022). https://doi.org/10.1007/s41605-022-00325-5
22. L. Huang, M. Huang, S. Xu et al., Intense Beam Issues in CSNS Accelerator Beam Commissioning, in *Proceedings of HB'23*, Geneva, Switzerland, MOA1I3, 16-22 (2023). https://doi.org/10.18429/JACoW-HB2023-MOA1I3
23. L. Huang, S. Wang, S. Xu et al., Sourceof instability in the rapid cycling synchrotron of the China Spallation Neutron Source. Eur. Phys. J. Plus **140**(1), 71 (2025). https://doi.org/10.1140/epjp/s13360-025-05997-8
24. H. Dong, H. Song, Q. Li et al., The vacuum system of the China spallation neutron source. Vacuum **154**, 75–81 (2018). https://doi.org/10.1016/j.vacuum.2018.04.046
25. D. Mohl, H. Song, Q. Li et al., On Landau Damping of dipole modes by nonlinear space charge and octupoles. Part. Acc. **50**, 177–187 (1995)
26. J. Gareyte, J. P. Koutchouk, F. Ruggiero, Landau damping, dynamic aperture and octupoles in LHC, CERN-LHC-Project-Report-91 (1997)
27. K.Y. Ng, *Physics of Intensity Dependent Beam Instabilities* (World Scientific, Singapore, 2006)
28. A. W. Chao, *Physics of Collective Beam Instabilities in High Energy Accelerators*. Wiley, New York, 15 (1993)
29. L. Huang, Y. Liu, S. Wang, Resistive wall instability in rapid Cycling synchrotron of China spallation neutron source. Nucl. Instrum. Methods Phys. Res. Sect. A. **728**, 1–5 (2013). https://doi.org/10.1016/j.nima.2013.06.017
30. S. Xu, S. Wang, Study of eddy current power loss in an RCS vacuum chamber. Chin. Phys. C **36**(2), 160–166 (2012). https://doi.org/10.1088/1674-1137/36/2/011
31. S. Wang, Y. An, S. Fang et al., An overview of design for CSNS/RCS and beam transport. Sci. China Phys. Mech. Astron. **54**(S2), 239–244 (2011). https://doi.org/10.1007/s11433-011-4564-x
32. C. Deng, Y. Liu, X. Wu et al., Transient simulation and field measurement of the trim quadrupoles and AC sextupoles for CSNS/RCS upgrade. IEEE Trans. Appl. Supercon. **32**(6), 4002605 (2022). https://doi.org/10.1109/TASC.2022.3151577
33. OPERA code, Available at https://www.3ds.com/products/simulia/opera, date last accessed July 29, (2024)
34. X. Wu, W. Kang, W. Chen et al., Design and performance of hall probe measurement system in CSNS. Radiat. Detect. Technol. Methods **1**(18), 1–5 (2017). https://doi.org/10.1007/s41605-023-00428-7
35. J. Zhou, W. Kang, S. Li et al., Development of rotating coil measurement system for China spallation neutron source. High Power Laser Part Beams **30**(10), 105101 (2018). https://doi.org/10.11884/HPLPB201830.180186
36. V. Kornilov, O. Boine-Frankenheim, Landau damping due to octupoles of non-rigid head-tail modes. Nucl. Instrum. Methods Phys. Res. Sect. A **951**, 163042 (2020). https://doi.org/10.1016/j.nima.2019.163042
37. V. Kornilov, O. Boine-Frankenheim, Space charge effects on Landau damping from octupoles, in *Proceedings of the ICFA mini-Workshop MCBI'19*, Zermatt, Switzerland, 237-241 (2019)
38. L. Huang, H. Liu, M. Li et al., Longitudinal dynamics study and optimization in the beam commissioning of the rapid cycling synchrotron in the China Spallation Neutron Source. Nucl. Instrum. Methods Phys. Res. Sect. A **998**, 165204 (2021). https://doi.org/10.1016/j.nima.2021.165204
39. V.H. Ranjbar, C.Y. Tan, Effect of impedance and higher order chromaticity on the measurement of linear chromaticity. Phys. Rev. Accel. Beams **14**, 082802 (2011). https://doi.org/10.1103/PhysRevSTAB.14.082802
40. W. Kang, L. Wang, L. Huo et al., Design and prototype test of CSNS/RCS injection and extraction magnets. IEEE Tran. Appl. Sup. **20**(3), 356–359 (2010). https://doi.org/10.1109/TASC.2010.2041756
41. X. Yang, T. Xu, S. Fu, Classical and modern power spectrum estimation for tune measurement in CSNS RCS. Chin. Phys. C **36**(7), 666–669 (2013). https://doi.org/10.1088/1674-1137/37/11/117003
42. S. Xu, S. Fang, S. Wang. Study on space charge effects of the CSNS/RCS, in *Proceedings of ICAP'09*, San Francisco, CA, USA, TH4IODN04, 239-244 (2009)